Nanoscale

Linking Melem with Conjugated Schiff-Base Bond to Boost Photocatalytic Efficiency of Carbon Nitride for Overall Water Splitting

Journal:	*Nanoscale*
Manuscript ID	NR-ART-03-2021-001940.R1
Article Type:	Paper
Date Submitted by the Author:	16-Apr-2021

Complete List of Authors:	Liu, Hu; Harbin Institute of Technology, School of Chemical Engineering and Technology Shen, Mengqi; Brown University, Chemistry Zhou, Peng; Wuhan University of Technology, Guo, Zhi; Shanghai Institute of Applied Physics, Chinese Academy of Science, Laboratory of Physical Biology Liu, Xinyang; Harbin Institute of Technology, Yang, Weiwei; Harbin Institute of Technology, Gao, Manyi; Harbin Institute of Technology Chen, Min; Brown University, School of Engineering Guan, Huanqin; Brown University Padture, Nitin; Brown University, School of Engineering Yu, Yongsheng; Harbin Institute of Technology, School of Chemistry and Chemical Engineering Guo, Shaojun; Peking University, Department of Materials Science and Engineering; Peking University, Department of Energy and Resources Engineering Sun, Shouheng; Brown University, Chemistry

Linking Melem with Conjugated Schiff-Base Bond to Boost Photocatalytic Efficiency of Carbon Nitride for Overall Water Splitting

Hu Liu[a,b,d†], Mengqi Shen[b†], Peng Zhou[c], Zhi Guo[e], Xinyang Liu[a], Weiwei Yang[a], Manyi Gao[a], Min Chen[f], Huanqin Guan[b], Nitin P. Padture[f], Yongsheng Yu[a*], Shaojun Guo[c*], Shouheng Sun[b*]

[a]MIIT Key Laboratory of Critical Materials Technology for New Energy Conversion and Storage, School of Chemistry and Chemical Engineering, Harbin Institute of Technology, Harbin, Heilongjiang 150001, China

[b]Department of Chemistry, Brown University, Providence, Rhode Island 02912, USA

[c]Department of Materials Science & Engineering, College of Engineering, Peking University, Beijing 100871, China

[d]School of Chemistry and Chemical Engineering, Xi'an University of Architecture and Technology, Xi'an 710055, China.

[e]Shanghai Synchrotron Radiation Facility. Shanghai Advanced Research Institute, CAS, Shanghai 201204, China

[f]School of Engineering, Brown University, Providence, Rhode Island 02912, USA

[†]H. Liu and M. Q. Shen contributed equally to this study.

AUTHOR INFORMATION

Corresponding Author

[*] Email: ysyu@hit.edu.cn;

[*] Email: guosj@pku.edu.cn;

[*] Email: ssun@brown.edu

ABSTRACT: Developing an efficient single component photocatalyst for overall water splitting under visible-light irradiation is extremely challenging. Herein, we report a metal-free graphitic carbon nitride (g-C_xN_4)-based nanosheet photocatalyst (x = 3.2, 3.6, or 3.8) with melem rings conjugated by Schiff-base bond (N=C-C=N). The presence of the conjugated Schiff-base bond tunes the band gap of g-C_xN_4 and, more importantly, serves as an electron sink to suppress electron-hole pair recombination. The projected density of states (PDOS) calculations suggest that the melem ring and Schiff-base bond act as oxidizing and reducing centers, respectively, for photocatalytic water splitting. As a result, g-C_xN_4, in particular g-$C_{3.6}N_4$, can catalyze overall water splitting without the need of any co-catalyst or sacrificial donor. Under visible light (>420 nm wavelength) irradiation, the g-$C_{3.6}N_4$ catalyzes the overall water splitting with H_2 and O_2 generation rates of 75.0 and 36.3 $\mu mol \cdot h^{-1} \cdot g^{-1}$, respectively. The g-$C_{3.6}N_4$ is the most efficient single-component photocatalyst ever reported for overall water splitting. Our studies demonstrate a new approach of tuning the bandgap and the electronic structure of graphitic carbon nitride for maximizing its photocatalysis for water splitting, which will be important for hydrogen generation and for energy applications.

Keywords:

Carbon nitride, Photocatalysis, Overall water splitting, Schiff-base bond, Metal-free

MAIN TEXT: The rapid increase in global energy demand and the need to build an energy-sustainable society are driving the extensive search for renewable energy[1]. Hydrogen (H_2) as an energy carrier has attracted great attention for replacing non-renewable fossil fuels due to its light weight and zero-carbon emission[2]. Among various methods developed to produce H_2, catalytic water splitting under sunlight is particularly appealing as a green-chemistry approach to sustainable energy[3-5]. Key to the success of this photocatalysis process is the development of efficient, *yet* low-cost and environmentally-friendly semiconductor catalysts, which can separate photogenerated electrons and holes for water reduction (to H_2) and oxidation (to O_2)[5,6]. To take full advantage of the solar energy for this

catalytic process, the catalyst must work under visible-light irradiation and have a band gap, E_g, in the range $1.8<E_g<3.0$ eV to promote water reduction/oxidation reactions at the catalyst surface[7-9].

Metal-based semiconducting catalysts have been studied extensively for photocatalytic water splitting. These catalysts require either dual photo-/electro-chemical power/co-catalysts[9-17], or acidic solution[18] in which metal leaching is inevitable. Thus, over the past decade or so, there have been extensive studies aimed at developing metal-free water-splitting photocatalysts that are not only more sustainable and stable, but also less expensive than the metal-based photocatalysts[19]. However, metal-free photocatalysts are usually inactive for overall water splitting in the absence of the co-catalyst or sacrificial donor[20.21] and can only work by its coupling with metal-based co-catalysts for good photocatalysis performance[22-31]. In this regard, the development of new strategies for promoting oxidizing and reducing activity of g-C_3N_4 to effectively catalyze overall water splitting without co-catalyst or sacrificial donor under visible-light irradiation is highly desirable, but still is extremely challenging.

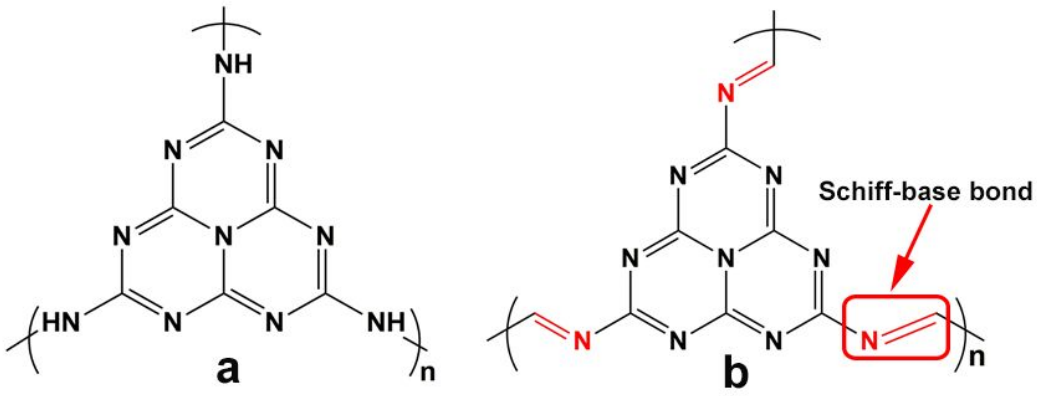

Scheme 1. Chemical structure of g-C_xN_4. (**a**) g-C_3N_4 and (**b**) g-$C_{3.6}N_4$, with the Schiff-base bond highlighted.

Here we report an efficient metal-free photocatalyst for overall water splitting with unprecedented catalysis performance under a visible-light (>420 nm) irradiation condition. The catalyst is based on g-C_3N_4 with its melem (2,5,8-triamino-tri-s-triazine) ring linked by glyoxal *via* conjugated Schiff-base bonds (N=C-C=N), forming g-C_xN_4 (**Scheme 1**), in which

x is controlled to be 3.2, 3.6, or 3.8. Among these g-C_xN_4, g-$C_{3.6}N_4$ shows the highest photocatalytic activity without any co-catalyst or sacrificial donor, owing to its efficient charge-carrier separation, outstanding visible-light absorption, and high density of active sites for water-molecule activation. Under visible light (>420 nm) irradiation, the g-$C_{3.6}N_4$ photocatalyzes overall water splitting with H_2 and O_2 generation rates of 75.0 and 36.3 $\mu mol \cdot h^{-1} \cdot g^{-1}$, respectively, which is the highest overall water splitting activity among all metal-free single component catalysts ever reported. The catalyst is also stable under visible-light photocatalytic conditions, showing no obvious activity drop after 120 h of continuous >420 nm light irradiation. Thus, g-$C_{3.6}N_4$ is a promising new metal-free photocatalyst for highly efficient overall water splitting.

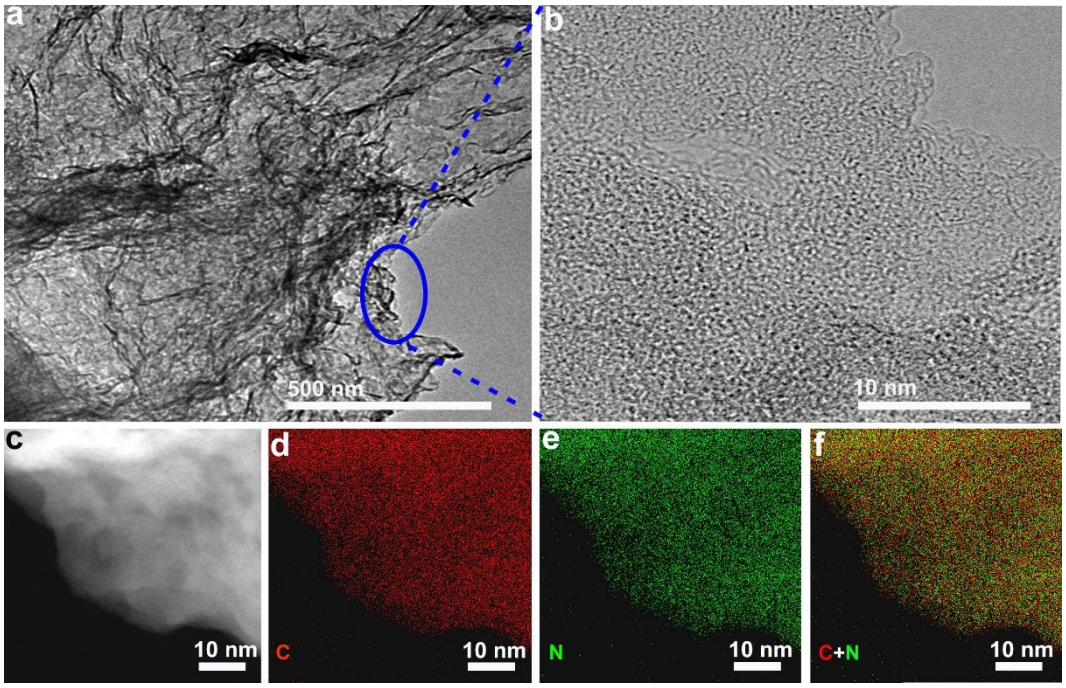

Figure 1. Microscopic characterization of g-$C_{3.6}N_4$. (**a**) TEM and (**b**) HR-TEM images. (**c**) HAADF-STEM image, and corresponding EDS elemental maps: (**d**) C, (**e**) N, and (**f**) combined C and N.

The g-C_xN_4 materials were synthesized by condensation of melamine and glyoxal using two-step heating, at 300 °C for 1 h followed by heating at 425 °C for 1 h, to form melem, which was further polymerized at 550 °C for 4 h (see details in the Methods section)[32]. In the g-C_xN_4 structure, x was controlled by varying the melamine-to-glyoxal molar ratio. X-ray photoelectron spectroscopy (XPS) and elemental analysis analyser were used to obtain the

carbon content (**Table S1&2**), and C-C/C=N percentage (**Table S3**), which was easily controlled by the amount of glyoxal added in the reaction process. **Figures 1a** and **1b** are the transmission electron microscopy (TEM) and high-resolution TEM (HR-TEM) images of a representative g-$C_{3.6}N_4$ nanosheet, which appears homogeneous and amorphous. High-angle annular dark-field scanning TEM (HAADF-STEM) and energy-dispersive X-ray spectroscopy (EDS) (**Figures 1c-1f**) show that C and N are distributed uniformly across the nanosheet. Our previous results about solid-state ^{13}C MAS NMR spectra of g-C_3N_4 and g-$C_{3.6}N_4$ show two peaks at 156.5 and 163.9 ppm corresponding to chemical shifts of C1 and C2 [32], respectively, in the melem ring[33,34], confirming that g-$C_{3.6}N_4$ still maintains the primary heptazine core structure of g-C_3N_4. A new peak at 148.5 ppm can be assigned to the chemical shift of C3 in the Schiff-base bond. Furthermore, C K-edge X-ray absorption near-edge spectroscopy (XANES) of g-$C_{3.6}N_4$ displays a new broad peak over 288.0-289.3 eV compared with that of g-C_3N_4, which is from the Schiff-base carbon atoms (**Figure S1**). Theoretical C K-edge XANES spectra (red dashed curve) of g-$C_{3.6}N_4$ calculated by Feff 9.7.1 match with the main spectral features of the experimental spectrum of g-$C_{3.6}N_4$ (**Figure S1**), further confirming the Schiff-base bonding to melem rings. As shown in N K-edge XANES spectra (**Figure S2**), the intensity of π* bond peak in g-$C_{3.6}N_4$ is stronger than that in g-C_3N_4, while the intensity of σ* bond peak is weaker, indicating a higher degree of π-conjugation in g-$C_{3.6}N_4$[31].

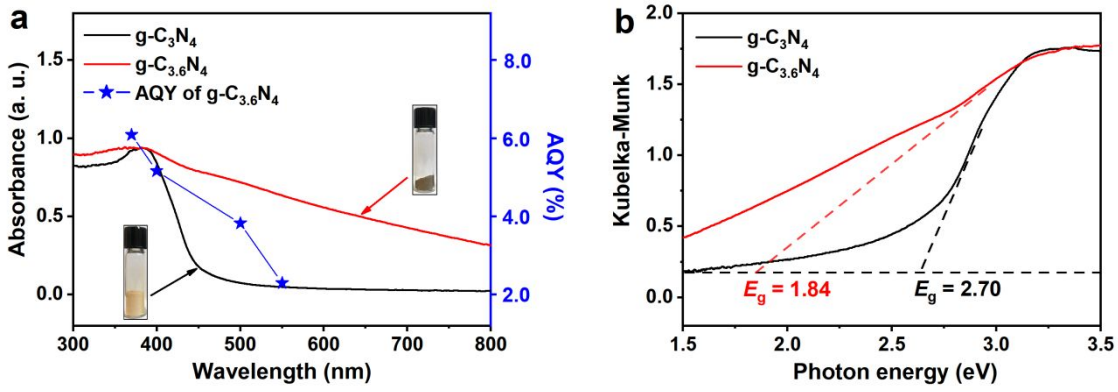

Figure 2. (**a**) UV-vis absorption spectra and (**b**) transformed Kubelka-Munk function plots of g-C_3N_4, and g-$C_{3.6}N_4$. In (**a**), the wavelength-dependent AQY of g-$C_{3.6}N_4$ highlighted by blue color in overall water splitting. In (**b**), the horizontal black dash line marks the baseline; the other dash lines are the tangents to the curves.

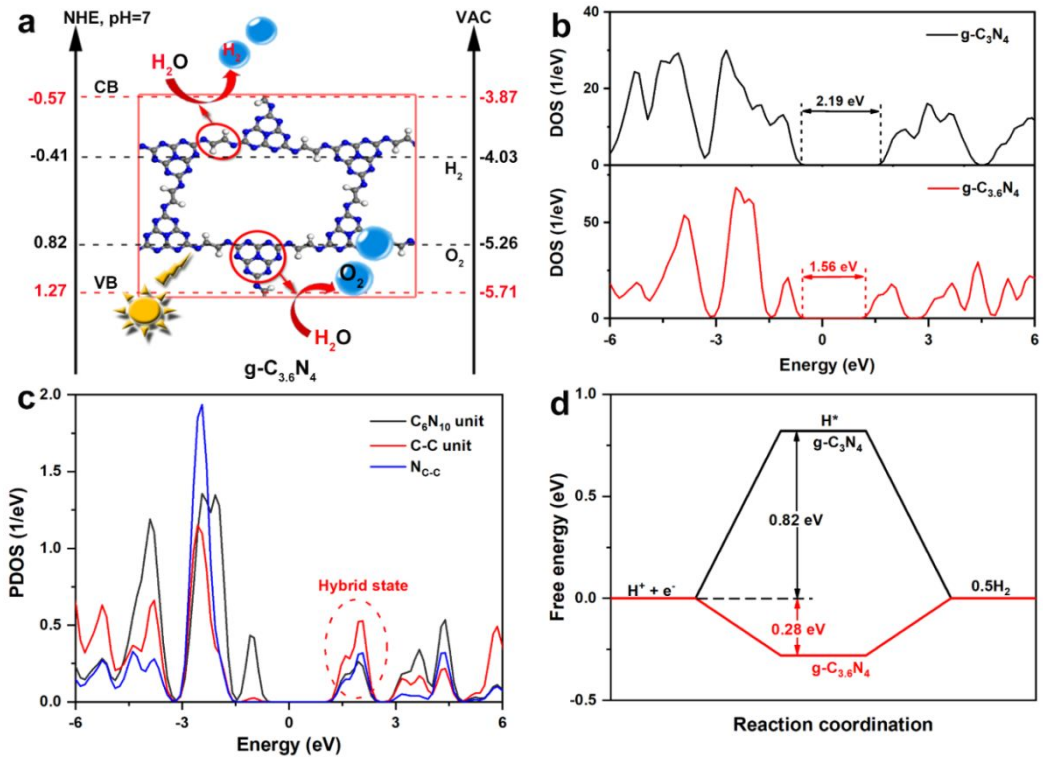

Figure 3. Electronic structure of g-C_xN_4. (**a**) Band-structure diagram of g-$C_{3.6}N_4$ calculated from optical absorption and electrochemical Mott-Schottky method. The top and bottom black dashed lines represent the H^+/H_2 and O_2/H_2O potentials, respectively. The top and bottom red dashed lines represent the CBM and VBM levels of g-$C_{3.6}N_4$, respectively. The melem ring (bottom) and Schiff-base bond (top) in the g-$C_{3.6}N_4$ structure act as oxidizing and reducing centers for overall photocatalytic water splitting, respectively. (**b**) Calculated band structures (DOS) of g-C_3N_4 (top) and g-$C_{3.6}N_4$ (bottom). (**c**) Calculated PDOS for the C_6N_{10} unit (black curve), C-C unit (red currve), and $N_{C\text{-}C}$ (blue curve). Note that C_6N_{10} unit is the melem ring, and C-C unit and $N_{C\text{-}C}$ are from the -N=C-C=N- group. (**d**) The calculated hydrogen adsorption energy of bridging N of g-C_3N_4 and g-$C_{3.6}N_4$ catalysts.

apparent quantum yield

UV-vis spectra (**Figures 2a&S3a**) show that the absorption intensities of the g-C_xN_4 are enhanced across the entire visible range by increasing the amount of Schiff-base bonds from x=3 to x=3.6, which is consistent with the color change from yellow to black (**Figure S4**). Correspondingly, the optical E_g values decrease from 2.7 to 1.84 eV (**Figures 2b&S3b**)[32]. The wavelength-dependent apparent quantum yield (AQY) of g-$C_{3.6}N_4$ was measured under the same photocatalytic reaction conditions by one-step excitation process, but different bandpass filters were used to provide monochromatic light for H_2 evolution in the overall

water splitting[33,34]. The AQY of g-$C_{3.6}N_4$ is 4.99% at 400 nm. Calculations using the electrochemical Mott-Schottky method[35] indicate that by increasing the amount of Schiff-base bonds in g-$C_{3.6}N_4$, the conduction-band minimum (CBM) and valence-band maximum (VBM) levels get closer to the H^+/H_2 and O_2/H_2O potentials, reaching -0.57 eV and 1.27 eV, respectively (*vs.* normal hydrogen electrode (NHE), *p*H=7) (**Figures 3a** and **S5**). This change is further supported by density of states (DOS) and projected density of states (PDOS) calculations. The DOS calculations result in somewhat lower E_g values of 2.19 eV and 1.56 eV for g-C_3N_4 and g-$C_{3.6}N_4$, respectively (**Figure 3b**). Nevertheless, the narrowing trend of E_g in g-$C_{3.6}N_4$ is attributed to the presence of conjugated Schiff-base bonds, in which C-C unit interacts with melem rings to produce a more negative hybrid state below the CB of g-C_3N_4 (**Figure 3c**). These calculations suggest that in g-$C_{3.6}N_4$, its CBM level is determined primarily by the Schiff-base group, while the VBM level is determined primarily by the melem ring. Thus, in the photocatalytic reaction, the photogenerated electrons from melem rings tend to be transferred to the Schiff-base group, leaving holes populated on the melem rings, resulting in beneficial electron-hole separation. Further calculation of the hydrogen-adsorption energy reveals that the N sites in the Schiff-base group show an optimized hydrogen-adsorption energy (-0.28 eV), as compared to the excessively positive hydrogen-adsorption energy (0.82 eV) on the N sites in g-C_3N_4, which facilitates hydrogen evolution reaction (HER) on g-$C_{3.6}N_4$ (**Figure 3d**). Compared with the N link in g-C_3N_4, the N=C-C=N link in g-$C_{3.6}N_4$ not only acts as a reducing center, but also extends the π-conjugation among the melem rings, narrowing the polymer E_g. Among the modified g-C_xN_4, g-$C_{3.6}N_4$ has more reducing/oxidizing centers than g-$C_{3.2}N_4$ due to the presence of more Schiff-base bonds (**Figure S6**).

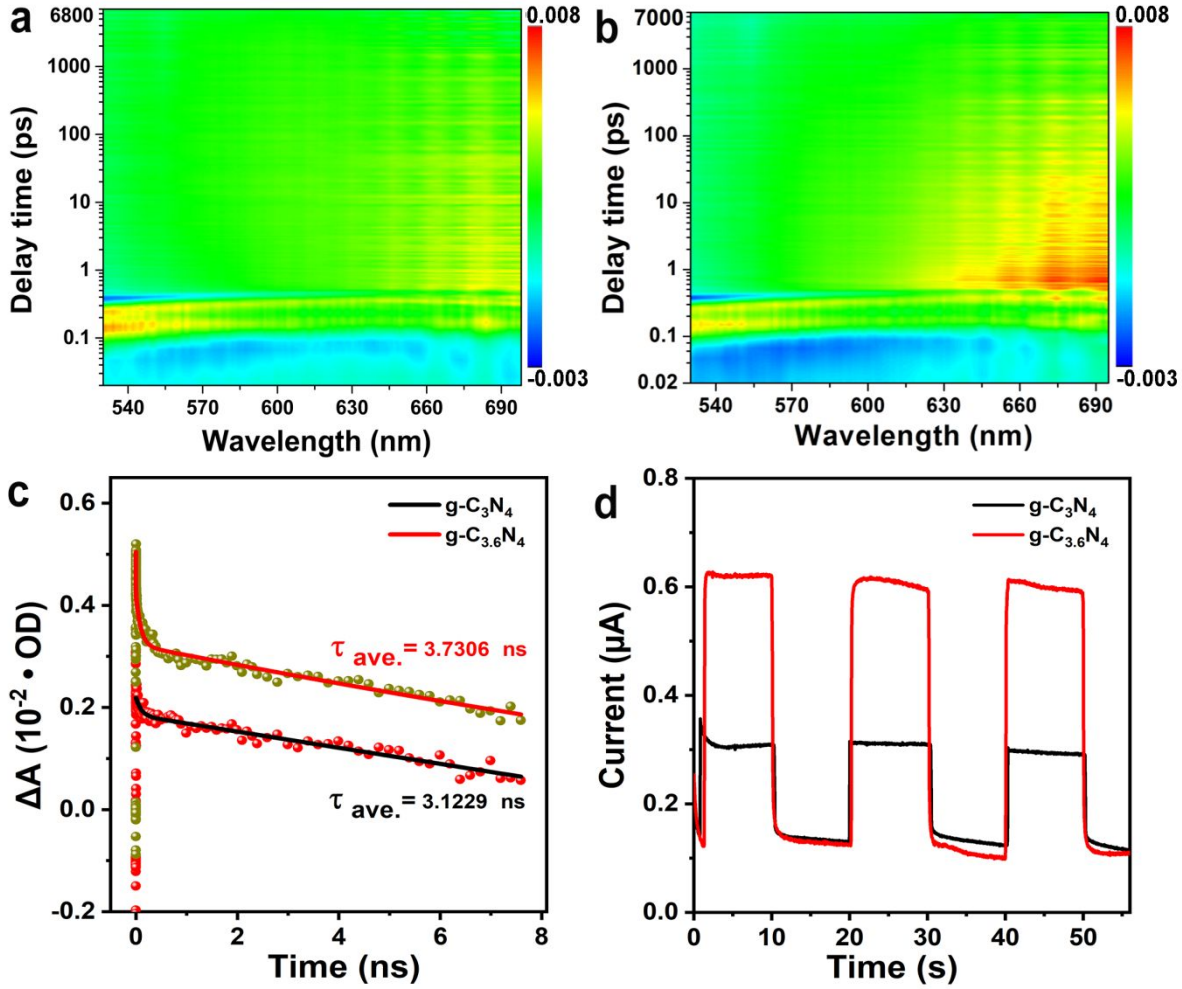

Figure 4. TAS results: (**a**) g-C_3N_4 and (**b**) g-$C_{3.6}N_4$. (**c**) The decay curves of g-C_3N_4 and g-$C_{3.6}N_4$ at 630 nm. (**d**) Photocurrent-potential curves for ITO/g-C_3N_4 and ITO/g-$C_{3.6}N_4$ at -1.0 V *vs.* Ag/AgCl in 0.5 M Na_2SO_4 exposed to visible light (λ>420 nm, 300 W Xe lamp).

The stabilization effect of the g-$C_{3.6}N_4$ structure on the photogenerated electrons and holes was characterized using transient absorption spectroscopy (TAS) to study hot-carrier relaxation in g-C_3N_4 and g-$C_{3.6}N_4$ films (see details in the Methods section). g-C_3N_4 has a fast carrier decay (<1 ps) at its absorption edge of 540 nm (**Figure 4a**), whereas g-$C_{3.6}N_4$ has a much slower absorption decay time (>10 ps) at its absorption edge of 680 nm (**Figure 4b**). The TAS spectrum also shows a characteristic feature of positive (ΔA>0) absorption change that can be attributed to the photoinduced absorption (PIA), and there is no significant change in the dynamics curves of g-C_3N_4 and g-$C_{3.6}N_4$ (**Figure S7**). Therefore, we choose dynamics data at 630 nm to calculate the carrier lifetime by two exponential decay function fitting of

the relaxation process. As shown in **Figure 4c**, g-$C_{3.6}N_4$ has a somewhat longer carrier average lifetime (3.7 ns) compared to that in g-C_3N_4 (3.1 ns). Similarly, **Figure S8** shows the spectra at time delays of 0 to 20 ps range, the decay signal for g-C_3N_4 and g-$C_{3.6}N_4$ was fitted by the two exponential decay function. The fitted time constants are listed in **Table S4**[36]. The result shows g-$C_{3.6}N_4$ has a somewhat longer carrier average lifetime compared to that in g-C_3N_4, indicating that the Schiff-base bonds enable more efficient separation of electrons and holes. This is further supported by the observation of a larger photocurrent response from g-$C_{3.6}N_4$ than from g-C_3N_4 (**Figure 4d**). These results suggest that compared to g-C_3N_4, g-$C_{3.6}N_4$ should be more efficient photocatalyst for overall water splitting.

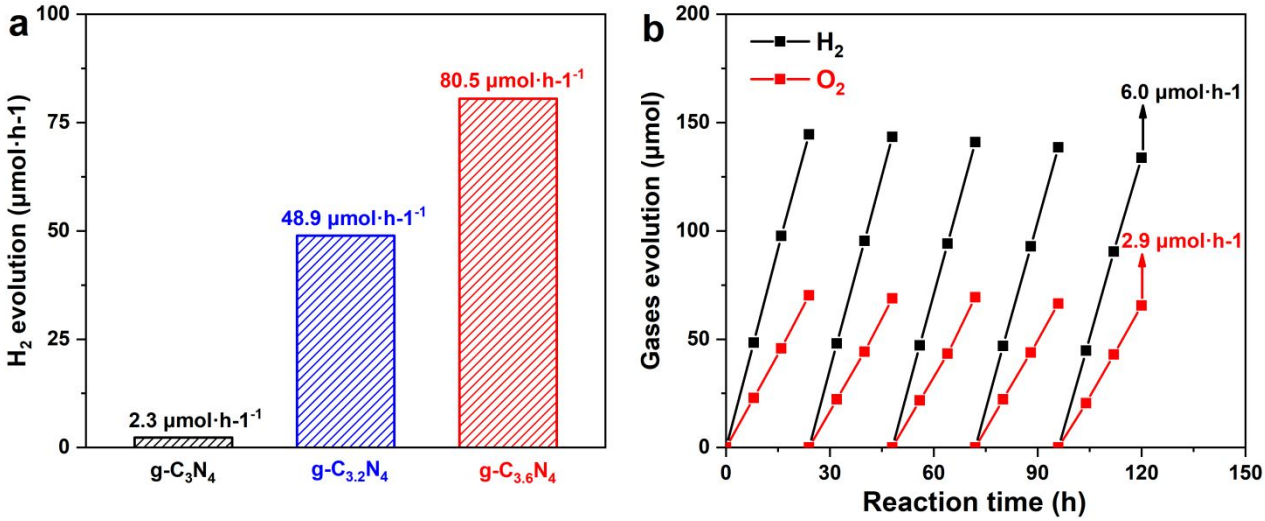

Figure 5. Photocatalytic water-splitting performance of g-C_xN_4. (**a**) Typical H_2 evolution from water under visible-light irradiation (300 W Xe lamp using a long-pass cutoff filter allowing wavelengths >420 nm) catalyzed by g-C_3N_4, g-$C_{3.2}N_4$ and g-$C_{3.6}N_4$. (**b**) Typical time course of H_2 and O_2 production from water under the visible-light irradiation photocatalyzed by g-$C_{3.6}N_4$.

We evaluated the photocatalytic water-splitting performance of the g-C_xN_4 dispersed in pure water. The evolving H_2 and O_2 gases mixture was characterized using a gas chromatograph (GC) (**Figures S9**). **Figure 5a** show the H_2 evolution rates from 100 mL of pure water containing 80 mg of g-C_3N_4, g-$C_{3.2}N_4$ or g-$C_{3.6}N_4$ photocatalyst under visible light (λ>420 nm). The g-$C_{3.2}N_4$ or g-$C_{3.6}N_4$ photocatalysts show enhanced hydrogen evolution over g-C_3N_4, the g-$C_{3.8}N_4$ is inactive for hydrogen evolution, the g-$C_{3.6}N_4$ shows the best

photocatalytic performance with a hydrogen generation rate of 80.5 μmol·h^{-1}, which is a 35-fold improvement over g-C_3N_4. We further measured the evolution of H_2 and O_2 from 100 mL of water containing 80 mg g-C_xN_4 under visible light irradiation (λ>420 nm) (**Figures 5b** and **S10**). Both g-$C_{3.2}N_4$ and g-$C_{3.6}N_4$ are active for overall water splitting, the g-$C_{3.8}N_4$ is also inactive under the same conditions due to its small band gap (<1.23 eV). The photocatalytic activity of g-$C_{3.6}N_4$ is improved 4-fold over g-$C_{3.2}N_4$, where the H_2 and O_2 generation rates are 75.0 and 36.3 μmol·h^{-1}·g^{-1}, respectively, with the H_2/O_2 molar ratio being close to the theoretical value of 2 for overall water splitting. These photocatalysis results are consistent with our theoretical analysis, confirming that Schiff-base bonds can indeed serve as reducing centers and the melem ring acts as the oxidizing center for overall water splitting. Compared with the reported metal-free photocatalyst, the single component g-$C_{3.6}N_4$ exhibits the most efficient photocatalytic activity for overall water splitting (**Table S5**). The g-$C_{3.6}N_4$ catalyst is not only active but also stable under photocatalytic condition, showing no noticeable catalysis deterioration after 120 h of continuous photocatalytic reaction (**Figure 5b**). The H_2 and O_2 evolution stopped immediately once the light was turned off, confirming that the H_2/O_2 evolution is originated from the light-induced catalysis.

In summary, we have reported a new strategy to tune the bandgap, the electronic structure, and photocatalytic properties of g-C_xN_4 nanosheets. By linking the melem ring with conjugated Schiff-base bond, polymeric g-C_xN_4 can be prepared with x = 3.2, 3.6, or 3.8. The conjugated Schiff-base bond present in the graphitic carbon nitride structure improves its visible-light adsorption, suppresses the electron-hole pair recombination, and serves as HER-active sites. The HER performance of the g-$C_{3.6}N_4$ (80.5 μmol h^{-1}) is ~35 times higher than that of the g-C_3N_4 (2.3 μmol h^{-1}). More importantly, this photocatalyst can generate H_2 and O_2 efficiently from pure water without the need of any co-catalysts and/or sacrificial donors. The g-$C_{3.6}N_4$-photocatalyzed overall water splitting generates H_2 and O_2 at the rates of 75.0 and 36.3 μmol·h^{-1}·g^{-1} (under >420 nm light irradiation), respectively. The g-$C_{3.6}N_4$ is the most efficient metal-free single component catalyst ever reported for overall water splitting. The melem conjugation strategy demonstrated here provides a new approach to enhance photocatalytic water splitting. The concept can be extended to connect melem ring

with different conjugation systems, making it possible to fine-tune the bandgap and electronic structure of graphitic carbon nitride to maximize its photocatalytic properties.

Supporting Information

Supporting Information is available from the Wiley Online Library or from the author.

Acknowledgements

This work was supported by the National Natural Science Foundation of China under Grant (No. 51871078 and 52071119) Heilongjiang Science Foundation (No. LH2020B006), Shaanxi Science Foundation (No. 2021JM-356) and Start-Up Funding for Class D Talent of Xi'an University of Architecture and Technology (No.1608720038). M. C. and N. P. P. acknowledge the research support from the US National Science Foundation (grant # OIA-1538893). The author is thankful for the support of BL02B of Shanghai Synchrotron Radiation Facility in the acquisition of NEXAFS data. The author also gratefully acknowledges financial support from the China Scholarship Council during a visit of Hu Liu to Brown University (No. 201706120320).

Author contributions

H. Liu and M. Q. Shen conceived the research and wrote the manuscript. H. Liu analyzed the water splitting performance. M. Q. Shen tested and analyzed the optical properties of carbon nitride. P. Zhou performed the DFT calculations, interpreted the catalytic mechanism and wrote the DFT calculations sections of the manuscript. X. Y. Liu helped with the carbon nitride synthesis. M. Y. Gao and H. Liu tested overall water splitting properties. Z. Guo. tested the K-edge XANES experimental spectra. W. W. Yang performed the TAS measurements. H. Q. Guan performed the ICP experiments. M. Chen and N. P. Padture helped with the optical measurements. Y. Y. Yu, S. J. Guo and S. H. Sun supervised the research. All authors discussed the results and contributed to the preparation of the manuscript.

Conflict of Interest

The authors declare no conflict of interest.

References

[1] M. Asif, and T. Muneer, *Renew. Sust. Energy Rev.*, **2007**, *11*, 1388-1413.

[2] L. Schlapbach, and A. Züttel, *Nature*, **2001**, *414*, 353-358.

[3] Z. Wang, C. Li, and K. Domen, *Chem. Soc. Rev.*, **2019**, *48*, 2109-2125.

[4] K. Maeda, K. Teramura, D. Lu, T. Takata, N. Saito, Y. Inoue, and K. Domen, *Nature*, **2006**, *440*, 295.

[5] T. Hisatomi, J. Kubota, and K. Domen, *Chem. Soc. Rev.*, **2014**, *43*, 7520-7535.

[6] A. Kudo, and Y. Miseki, *Chem. Soc. Rev.*, **2009**, *38*, 253-278.

[7] S. Chen, T. Takata, and K. Domen, *Nat. Rev. Mater.*, **2017**, *2*, 1.

[8] P. Z. Chen, K. Xu, T. P. Zhou, Y. Tong, J. C. Wu, H. Cheng, X. L. Lu, H. Ding, C. Z. Wu, and Y. Xie, *Angew. Chem. Int. Ed.*, **2016**, *55*, 2488-2492.

[9] S. J. Moniz, S. A. Shevlin, D. J. Martin, Z. X. Guo, and J. Tang, *Energy Environ. Sci.*, **2015**, *8*, 731-759.

[10] Z. Wang, Y. Inoue, T. Hisatomi, R. Ishikawa, Q. Wang, T. Takata, S. Chen, N. Shibata, Y. Ikuhara and K. Domen, *Nat. Catal.*, **2018**, *1*, 756-763.

[11] L. Liao, Q. Zhang, Z. Su, Z. Zhao, Y. Wang, Y. Li, X. Lu, D. Wei, G. Feng, Q. Yu, X. Cai, J. Zhao, Z. Ren, H. Fang, F. Robles-Hernandez, S. Baldelli and J. Bao, *Nat. Nanotech.*, **2014**, *9*, 69-73.

[12] J. Kondo, *Chem. Commun.*, **1998**, *3*, 357-358.

[13] K. Maeda, K. Teramura, D. Lu, N. Saito, Y. Inoue, and K. Domen, *Angew. Chem. Int. Ed.*, **2006**, *45*, 7806-7809.

[14] K. Maeda, T. Takata, M. Hara, N. Saito, Y. Inoue, H. Kobayashi, and K. Domen, *J. Am. Chem. Soc.*, **2005**, *127*, 8286-8287.

[15] X. Yang, A. Wolcott, G. Wang, A. Sobo, R. C. Fitzmorris, F. Qian, and Y. Li, *Nano Lett.*, **2009**, *9*, 2331.

[16] M. Chen, J. Gu, C. Sun, Y. Zhao, R. Zhang, X. You, Q. Liu, W. Zhang, Y. Su, H. Su, and D. Zhang, *ACS Nano*, **2016**, *10*, 6693-6701.

[17] X. Wang, Q. Xu, M. Li, S. Shen, X. Wang, Y. Wang, Z. Feng, J. Shi, H. Han, and C. Li, *Angew. Chem. Int. Ed.*, **2012**, *124*, 13266-13269.

[18] A. Fujishima, and K. Honda, *Nature*, **1972**, *238*, 37-38.

[19] Y. Xu, M. Kraft, and R. Xu, *Chem. Soc. Rev.*, **2016**, *45*, 3039-3052.

[20] X. Wang, K. Maeda, A. Thomas, K. Takanabe, G. Xin, J. M. Carlsson, and M. Antonietti, *Nat. Mater.*, **2009**, *8*, 76-80.

[21] H. Wang, X. D. Zhang, and Y. Xie, *Mater. Today*, **2019**, *23*, 72-86.

[22] P. Zhou, F. Lv, N. Li, Y. Zhang, Z. Mu, Y. Tang, and S. Guo, *Nano energy*, **2019**, 56, 127-137.

[23] X.Wang, C. Zhou, R. Shi, Q. Liu, G. I. Waterhouse, L. Wu, and T. Zhang, *Nano Research*, **2019**, 12, 2385-2389..

[24] C. Zhou, R. Shi, L. Shang, L. Z. Wu, C. H. Tung, and T. Zhang, *Nano Research*, **2018**, 11, 3462-3468.

[25] D. Wang, H. Zeng, X. Xiong, M. F. Wu, M. Xia, M. Xie, and S. L. Luo, *Science Bulletin*, **2020**, 65, 113-122..

[26] B. Zhu, B. Cheng, L. Zhang, J. Yu, *Carbon Energy*, **2019**, 1, 32-56.

[27] J. Li, D. Wu, J. Iocozzia, H. Du, X. Liu, Y. P. Yuan, W. Zhou, Z. Lin, Z. M. Xue, and Z. Q. Lin, *Angew. Chem. Int. Ed.*, **2019**, *131*, 2007-2011.

[28] Y. Tang, P. Zhou, Y. Chao, F. Lin, J. Lai, H. Li, and S. Guo, *Science China Materials*, **2019**, 62, 351-358..

[29] S. Cao, J. Low, J. Yu, and M. Jaroniec, *Adv. Mater.*, **2015**, *27*, 2150-2176.

[30] G. Zhang, Z. A. Lan, L. Lin, S. Lin, and X. Wang, *Chem. Sci.*, **2016**, *7*, 3062-3066.

[31] J. Liu, Y. Liu, N. Liu, Y. Han, X. Zhang, H. Huang, Y. Lifshitz, S. T. Lee, J. Zhong, and Z. Kang, *Science*, **2015**, *347*, 970-974.

[32] H. Liu, X. X. Li, X. Y. Liu, Z. H. Ma, Z. Y. Yin, W. W. Yang, and Y. S. Yu, *Rare Met.*, **2021**, 2021, 40, 808-816.

[33] D. Zhao, Y. Wang, C. L. Dong, Y. C. Huang, J. Chen, F. Xue, and L. Guo, *Nature Energy*, **2021**, 1-10.

[34] Y. R. Li, T. T. Kong, and S. H. Shen, *Small*, **2019**, *15*, 1900772.

[35] G. Zhang, Z. A. Lan, and X. Wang, *Chem. Sci.*, **2017**, *8*, 5261-5274.

[36] M. A. Khan, P. Maity, M. Al-Oufi, I. K. Al-Howaish, and H. Idriss, *J. Phys. Chem. C*, **2018**, 122, 16779-16787.